JACS
JOURNAL OF THE AMERICAN CHEMICAL SOCIETY
Article
pubs.acs.org/JACS

Filming the Birth of Molecules and Accompanying Solvent Rearrangement

Jae Hyuk Lee,[†] Michael Wulff,*[,‡] Savo Bratos,[§] Jakob Petersen,[⊥] Laurent Guerin,[‡,○] Jean-Claude Leicknam,[§] Marco Cammarata,[‡,○] Qingyu Kong,[#] Jeongho Kim,[†,∥] Klaus B. Møller,[⊥] and Hyotcherl Ihee*[,†,▽]

[†]Center for Time-Resolved Diffraction, Department of Chemistry, KAIST, Daejeon 305-701, Republic of Korea

[‡]European Synchrotron Radiation Facility, BP 220, 38043 Grenoble Cedex, France

[§]Laboratoire de Physique Théorique de la Matière Condensée, Université Pierre et Marie Curie, Case Courrier 121, 4 Place Jussieu, 75252 Paris Cedex 05, France

[∥]Department of Chemistry, Inha University, Incheon, 402-751, Republic of Korea

[⊥]Centre for Molecular Movies, Department of Chemistry, Technical University of Denmark, Kemitorvet 207, 2800 Kgs. Lyngby, Denmark

[#]Synchrotron Soleil, L'Orme des Merisiers, Saint-Aubin, BP 48, 91192 Gif-sur-Yvette Cedex, France

[▽]Center for Nanomaterials and Chemical Reactions, Institute for Basic Science, Daejeon 305-701, Republic of Korea

Supporting Information

ABSTRACT: Molecules are often born with high energy and large-amplitude vibrations. In solution, a newly formed molecule cools down by transferring energy to the surrounding solvent molecules. The progression of the molecular and solute−solvent cage structure during this fundamental process has been elusive, and spectroscopic data generally do not provide such structural information. Here, we use picosecond X-ray liquidography (solution scattering) to visualize time-dependent structural changes associated with the vibrational relaxation of I_2 molecules in two different solvents, CCl_4 and cyclohexane. The birth and vibrational relaxation of I_2 molecules and the associated rearrangement of solvent molecules are mapped out in the form of a temporally varying interatomic distance distribution. The I−I distance increases up to ∼4 Å and returns to the equilibrium distance (2.67 Å) in the ground state, and the first solvation cage expands by ∼1.5 Å along the I−I axis and then shrinks back accompanying the structural change of the I_2 molecule.

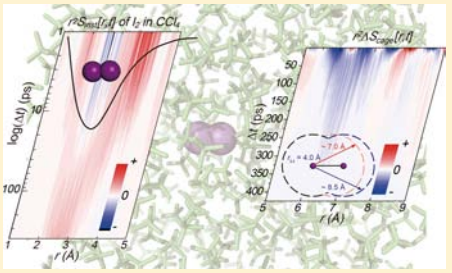

1. INTRODUCTION

The solvent plays an important role in solution-phase chemical reactions by serving as an energy source to activate the reaction as well as a heat bath to stabilize the products. As a result, the properties of the solvent significantly affect the energy landscape, rates, and pathways of a reaction in solution. The interplay of solute and solvent molecules and its effect on the outcome of chemical reactions have been a topic of intense research in the field of reaction dynamics over several decades, and the kinetic and spectral signatures of the solvation process have been elucidated on femto- to picosecond time scales.[1−4] However, despite these efforts, it is still challenging to experimentally probe the solvation response associated with a chemical reaction, especially the rearrangement of solute−solvent configuration accompanying the structural change of reacting solute molecules, mainly due to the lack of tools that have both time resolution and structural sensitivity. In this work, we apply time-resolved X-ray liquidography (solution scattering) to the geminate recombination and vibrational relaxation processes of iodine (I_2) in solution and probe the motions of solute molecules and the solute−solvent cage in real time.

Geminate recombination of iodine atoms to form molecular I_2 in solution after photodissociation is a good example of a prototype solution-phase reaction and it has been investigated by spectroscopy and quantum chemistry for more than seven decades.[5−25] This reaction occurs due to collisions of a dissociating I_2 molecule with the surrounding solvent molecules, whereby the vibrational kinetic energy of the I_2 molecule is dissipated as the molecule reaches thermal equilibrium.[11−13] The dynamics of vibrational energy dissipation has been well characterized by spectroscopic studies of the photodissociation and subsequent recombination of I_2 in CCl_4, alkane liquids, and noble gas matrices.[8,14−25] However, the change in molecular structure (i.e., bond length change) and the response of the surrounding solvent cage have never been directly observed. Time-resolved X-ray liquidography[26−47]

Received: December 21, 2012
Published: February 1, 2013

is well suited for monitoring this solution-phase reaction because it directly probes the interatomic distance distribution as a function of time. However, due to the rather long pulse (~100 ps) of a synchrotron X-ray pulse, the vibrational cooling process of I_2 in solution has not been visualized in real space so far. Here, we present a new synchrotron experiment that remedies the situation by using the time-slicing scheme where data are collected at earlier time delays and with finer time increments (down to 10 ps) than the X-ray pulse width (Figure 1b). Combined with deconvolution data processing, we extract

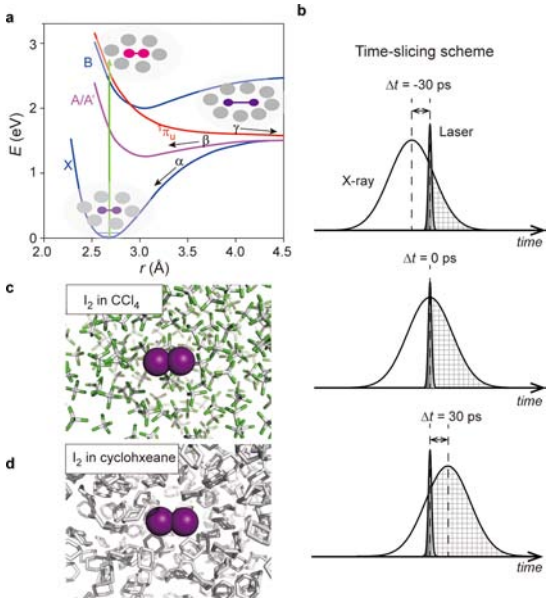

Figure 1. (a) Potential energy surfaces of low-lying electronic states (X, A/A′, B, and $^1\pi_u$) of I_2. The states A and A′ are closely spaced and can be viewed as a single electronic state A/A′. The processes α and β represent geminate recombination of two I atoms in the X and A/A′ states, respectively. The process γ represents nongeminate recombination through the solvent. Schematic snapshots of the solute−solvent configuration at representative stages are depicted. (b) Schematic of the time-slicing experiment. At a negative time delay (for example −30 ps) close to time zero, the X-ray pulse arrives (effectively) earlier than the laser pulse, but the X-ray pulse, which is much longer than the laser pulse, is still present after the interaction with the laser pulse and thus scattered off the laser-illuminated sample. At time zero, half of the X-ray pulse probes the laser-illuminated sample. At a positive time delay, most of the X-ray pulse is scattered off the laser-illuminated sample. (c) Molecular dynamics (MD) snapshot of I_2 in CCl_4. The purple sphere is an iodine atom, the gray rod is a carbon atom, and the green rod is a chloride atom. (d) MD snapshot of I_2 in cyclohexane. The purple sphere is an iodine atom, and the gray rod is a carbon atom.

the dynamics that occur faster than the X-ray pulse width and monitor the evolution of not only the interatomic distance distribution of iodine atoms in CCl_4 (Figure 1c) and cyclohexane (Figure 1d) but also the solute−solvent distance distribution at the early stages of I−I bond formation in CCl_4.

2. METHODS

The experiments were performed on beamline ID09B at the European Synchrotron Radiation Facility in Grenoble. A typical pump−probe scheme with optical pump and X-ray probe pulses was adopted to initiate and monitor the chemical reaction of interest. The solution sample was prepared by dissolving I_2 (Sigma−Aldrich, PN I8780, 99.2%) in CCl_4 (Sigma−Aldrich, PN 270652, 99.9%) or cyclohexane (Sigma−Aldrich, PN 676861, ≥ 99%) at 25 mM or 20 mM concentration, respectively, and circulated through a high-pressure slit nozzle (0.3 mm slit, Kyburz) to form a liquid jet. The optical excitation was realized with laser pulses at 530 nm (for I_2 in CCl_4) or 520 nm (for I_2 in cyclohexane). The scattering was recorded on an integrating CCD detector with fast readout (FReLoN camera, 2048 pixel × 2048 pixel, detection area 105 × 105 mm^2, and readout to 16 bits in 0.5 s per image). Scattering patterns probing the I_2 recombination were collected as a function of the pump−probe delay t from −200 to 400 ps with a time step of 10 ps. The signal at a negative time delay, $S(q, -3\ \text{ns})$, was subtracted from the signals at other delays, $S(q, t)$, to obtain the difference signals, $\Delta S(q, t)$. More details on the experimental procedures, data processing, and molecular dynamics (MD) simulations are given in the Supporting Information.

3. RESULTS AND DISCUSSION

3.1. Photochemistry of I_2 in Solution and the Time-Slicing Scheme. In the experiment, the solution sample is pumped by picosecond optical laser pulses, promoting a fraction of I_2 molecules from the ground state X to the excited electronic states B and $^1\pi_u$ (Figure 1a). Excited I_2 molecules in the solvent cage dissociate rapidly and form an activated complex $(I_2)^*$ with an elongated bond length. A fraction of the $(I_2)^*$ complexes escape the cage and recombine nongeminately in tens of nanoseconds.[48] The remaining $(I_2)^*$ complexes recombine geminately along either the X or A/A′ potential energy surface while exhibiting large-amplitude vibrations. These vibrational relaxation processes were monitored by time-delayed, 100 ps X-ray pulses from a synchrotron.

Scattering patterns containing a fingerprint of the I_2 recombination were collected as a function of the pump−probe delay t from −200 to 400 ps with a time step of 10 ps. As the optical pulses (0.5 ps) are much shorter than the X-ray pulses (100 ps), at early time delays between −100 and 100 ps, the signal from the photoexcited sample is produced only by the part of the X-ray pulse that arrives after the laser pulse (Figure 1b). For example, at zero time delay, the laser pulse is temporally located in the middle of the X-ray pulse, and the excited sample is probed only by the truncated half of the Gaussian X-ray intensity. The signal at a negative time delay, $S(q, -3\ \text{ns})$, was subtracted from the signals at other delays, $S(q, t)$, to obtain the difference scattering signals, $\Delta S(q, t)$. The Fourier transform of the difference scattering, $\Delta S[r, t]$, is a measure of the change in the electron density, from which the changes in the I−I distance distributions and the solute−solvent cage structure are inferred. The solvent is unavoidably heated by the recombining I atoms, giving rise to a thermal signal. By suitable scaling of the solvent response to an ultrafast temperature jump, the contribution from solvent heating was removed (see the Supporting Information).[28,38] To maximize the X-ray intensity, the raw quasi-monochromatic beam, which has an asymmetric energy spectrum with 3% bandwidth, from the undulator fundamental was used. The polychromaticity in the spectrum leads to a slight shift and damping in the scattered intensity $\Delta S(q)$ and its Fourier transform $\Delta S[r]$, and the distortion of the signal was corrected as shown in the Supporting Information. Note that we multiply $S[r]$ by r^2 because $r^2S[r]$ is directly related with the radial distribution function, $\rho(r)$, as described in the Supporting Information. From now on, we define $r^2S[r]$ as a distance distribution function.

3.2. Sharpening the Signal by Deconvolution. The measured difference signal $r^2\Delta S[r, t]$ is the convolution of the instantaneous response of the sample, $r^2\Delta S_{inst}[r, t]$, and the profile of X-ray pulse intensity, $I_{X\text{-}ray}(t)$ obtained by streak-

camera measurements.[49,50] While $r^2\Delta S_{inst}[r, t]$ contains the desired information on the bond formation dynamics of I_2, the measured signal $r^2\Delta S[r, t]$ is slightly blurred by the effect of the X-ray pulse that has a finite temporal width. Therefore, one needs to deconvolute the X-ray pulse profile from $r^2\Delta S[r, t]$ to correct for the finite pulse width. There are several deconvolution algorithms available: constrained iteration, inverse filter, and least-mean-square algorithms.[51−53] The last method was mainly used in this work as detailed in the Supporting Information. We also tested the constrained iteration algorithm to check the method dependence of the deconvoluted signals, and the results confirm that the same result is obtained within experimental errors regardless of the deconvolution methods (Supporting Information, Figure S17). Along with the deconvolution, a series of data processing procedures were employed to extract the structural changes more clearly. To assess the reliability of the used procedures, we applied the exact same procedures to mock data and examined the uncertainties introduced by the procedures. From this test, we confirmed that our procedures are reliable with a spatial uncertainty of ∼0.06 Å and temporal uncertainty of ∼10 ps (see the Supporting Information).

While time-dependent changes of the measured signal are already distinct in $r^2\Delta S[r, t]$ (Supporting Information, Figure S7a) without deconvolution, they are enhanced in the deconvoluted $r^2\Delta S_{inst}[r, t]$ curves (Figure 2a for I_2/CCl_4 and Figure 2b for I_2/cyclohexane). In I_2/CCl_4, the negative peak at ∼2.67 Å, which corresponds to the depletion of I_2 in the ground state, is visible for all time delays, but its magnitude gradually becomes smaller with time as the ground state is repopulated. At early time delays up to 26 ps, positive peaks at distances above 4 Å are visible, but their magnitudes rapidly decay. At later time delays, only one positive peak around ∼3.1 Å, which we assign to the equilibrium A/A′ state (see below), remains, and its magnitude decreases slowly with time. Although the equilibrium I−I distances in the X and A/A′ states are 2.67 and 3.1 Å, respectively, the positions of the negative and positive peaks are slightly shifted from these values in the difference curves. This peak shift is due to a partial overlap of positive and negative peaks. In Figure 2a,b, the slight oscillation in the high r region is an artifact caused by the limited q range used in the Fourier transform. The period of this oscillation is $2\pi/q_{max}$, where q_{max} is the maximum q used in the Fourier transform. In our case, q_{max} is 9 Å^{-1}, and thus, the period is ∼0.7 Å.

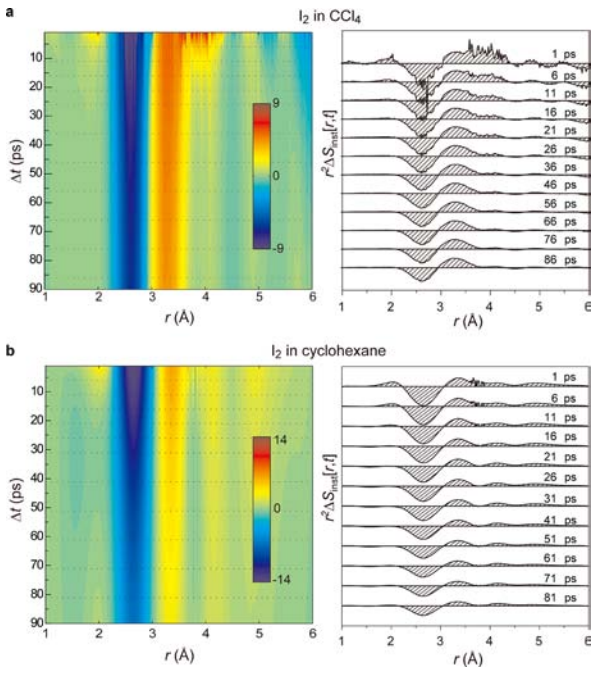

Figure 2. Deconvoluted difference distance distribution ($r^2\Delta S_{inst}[r, t]$) of I_2 formation. (a) Difference X-ray scattering signal $r^2\Delta S_{inst}[r, t]$ with the X-ray pulse profile deconvoluted (left) and their cross sections at various time delays (indicated by dotted lines in the left figure) for I_2 in CCl_4. (b) Difference X-ray scattering signal $r^2\Delta S_{inst}[r, t]$ with the X-ray pulse profile deconvoluted (left) and their cross sections at various time delays (indicated by dotted lines in the left figure) for I_2 in cyclohexane.

In principle, $r^2\Delta S_{inst}[r, t]$ reflects the motions of iodine atoms in the two electronic states X and A/A′. However, there is already a distinct peak at ∼3.1 Å corresponding to equilibrium A/A′, even at the earliest time delays, suggesting that the relaxation in the A/A′ state is completed within our limited time resolution imposed by the 10 ps increment of the time delay. This is supported by the fact that no further growth of the ∼3.1 Å peak is observed. The A/A′ state has a rather long lifetime compared with the time range investigated in this measurement. In addition, a small fraction of I_2 completely dissociates into iodine atoms and do not return to I_2 in the investigated time range. To remove the contribution from these long-lived states, double difference signals, $r^2\Delta\Delta S_{inst}[r, t] = r^2\Delta S_{inst}[r, t] - r^2\Delta S_{inst}[r, t_\infty]$, were calculated, where t_∞ is a time delay (426 ps here) much longer than the time taken for vibrational relaxation in the X state.

In I_2/cyclohexane, the deconvoluted signals show quite different behavior compared to I_2/CCl_4. As in I_2/CCl_4, the negative peak at ∼2.67 Å (depletion of I_2 in the ground state) and the positive peak at ∼3.1 Å (A/A′ state) are observed, and positive peaks at distances larger than 4 Å are also visible. However, the positive peak at ∼3.1 Å decays much faster than in I_2/CCl_4, indicating strong solvent dependence of the lifetime of the A/A′ state. As reported by Harris et al.,[16] in cyclohexane, the decay of A/A′ state occurs on the same time scale as the vibrational cooling process. For this reason, in cyclohexane, the decay of the A/A′ state and vibrational cooling cannot be distinguished from each other in the deconvoluted signal, $r^2\Delta S_{inst}[r, t]$. The positive peak at ∼3.1 Å (A/A′ state) is noticeably smaller in cyclohexane than in CCl_4, indicating that the A/A′ state is relatively less populated in cyclohexane. This observation is consistent with previous spectroscopic studies.[17]

3.3. Time-Dependent Distance Distribution. Finally, using the relationship $r^2S_{inst}[r, t] = r^2\Delta\Delta S_{inst}[r, t] + r^2S_{I2,X}[r]$, we remove the negative peak at 2.67 Å corresponding to the depletion of ground-state I_2 ($r^2S_{I2,X}[r]$) in CCl_4 and extracted the I−I distance distribution $r^2S_{inst}[r, t]$ arising from only recombining iodine atoms in the cage as shown in Figure 3a,b. The I−I distance distribution vividly visualizes the time-dependent progression of the I−I distance. At early times, the positive peak at ∼4 Å with a large width is clearly visible. At later time delays, the peak shifts to shorter distances and eventually only one sharp positive peak remains around 2.67 Å, representing the equilibrium X state. To quantify the shift of the peak, we calculate the average distance $<r(t)>$ as a function of time by averaging the data from 1.5 to 4.5 Å as shown in Figure 3c. The $<r(t)>$ converges to 2.67 Å, the equilibrium I−I distance of the X state. The temporal decay profile is fit well by

dx.doi.org/10.1021/ja312513w | J. Am. Chem. Soc. 2013, 135, 3255−3261

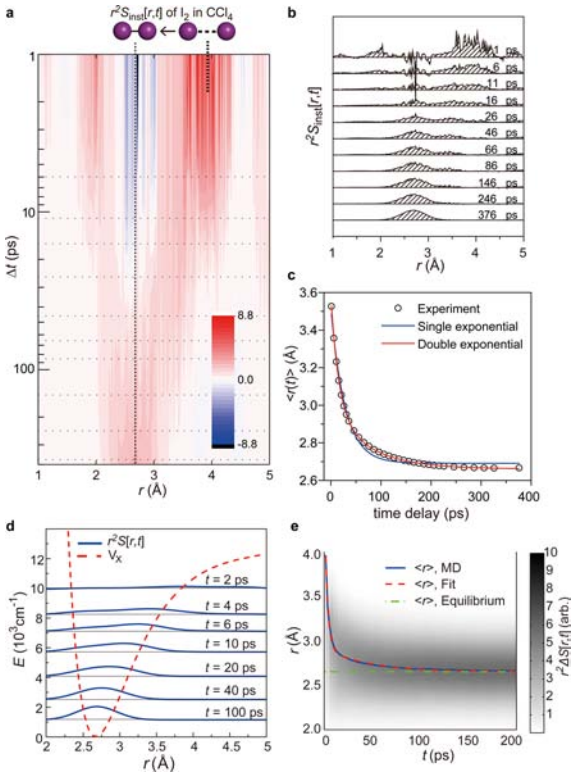

Figure 3. Time-dependent distance distribution functions ($r^2S_{inst}[r, t]$) of I_2 in CCl_4. (a) The $r^2S_{inst}[r, t]$ curves corresponding to time-dependent I–I distance distribution functions of I_2 in CCl_4. (b) Cross sections of $r^2S_{inst}[r, t]$ at the time delays indicated by dotted lines in (a). (c) Time evolution of the average I–I distance $<r(t)>$ was calculated from (a) and compared with a single-exponential fit (blue) and a double-exponential fit (red). To obtain a satisfactory fit to the experimental data, a double exponential is necessary with the time constants of 16 and 76 ps and a relative amplitude ratio of about 2:1. (d) Time evolution of the I–I distance distribution function $r^2S[r, t]$ converted from $\rho(r, t)$ (blue, solid line) of the I–I atomic pair obtained by MD simulation. The potential energy curve corresponding to the X state is also shown (red, dashed line). (e) Time dependence of the distance distribution function $r^2S[r, t]$. Fit of the average distance $<r>$ (blue, solid line) to a biexponential function (red, dashed line) gives the relaxation times of 3 and 44 ps. The equilibrium distance (green, dash-dotted line) is also shown.

a double-exponential function with time constants of 16 and 76 ps. In fact, a single-exponential function does not give a satisfactory fit while adding more exponential components does not improve the fit. Therefore, the vibrational cooling in the X state can be described by a biexponential process. This biexponential decay and the general time-dependent change of the distance distribution are also supported by MD simulations. In Figure 3d (also in Figure S18a in the Supporting Information), the time evolution of the distribution function $r^2S_{inst}(r, t)$ of the I–I atomic pair obtained from the MD simulation is shown. The spread of $r^2S_{inst}(r, t)$ decreases with time as the ensemble of I_2 molecules relaxes toward the bottom of the potential well of the X state. As seen in Figure 3e (also in Figure S18c of the Supporting Information), the decay of the average I–I distance $<r>$ is well fit by a biexponential function, in agreement with the biphasic decay observed in the experimental data.

The biexponential dynamics of the vibrational relaxation for I_2 in CCl_4 found in this study provides an explanation for the result of a previous ultrafast spectroscopic study.[8] In that study, the decay of vibrational energy monitored from 50 to 200 ps shows single-exponential dynamics, but our biexponential behavior can be inferred indirectly. The vibrational energy decays from 2000 cm^{-1} at 50 ps to 300 cm^{-1} at 200 ps, and the decay profile was fit with an exponential of 70 ps time constant in agreement with the time constant of the slower component in our measurement. Although the time range corresponding to a faster decay component was not investigated in that study, considering that the well depth of the X state is 12 000 cm^{-1}, the vibrational energy must have decayed by 10 000 cm^{-1} within the first 50 ps (Supporting Information, Figure S18b). Therefore, this component should correspond to the first time constant of 16 ps obtained in our study.

In the same manner as for the I_2/CCl_4 data, the negative peak for the ground-state I_2 was removed from the cyclohexane data to give the distance distribution $r^2S_{inst}[r, t]$ arising from only recombining iodine atoms as shown in Figure 4a,b. As in

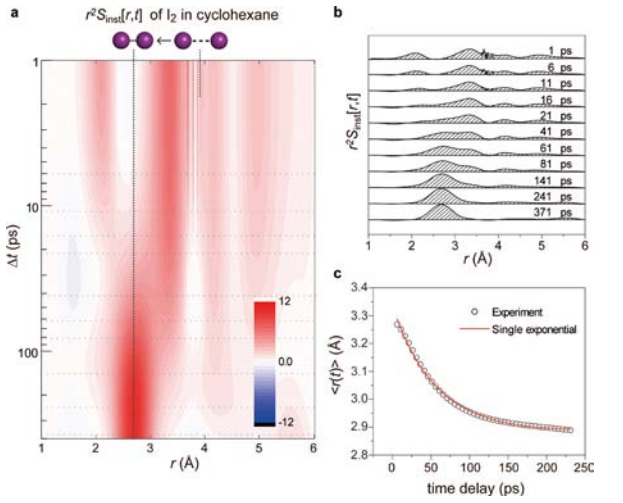

Figure 4. Time-dependent distance distribution functions ($r^2S_{inst}[r, t]$) of I_2 in cyclohexane. (a) The $r^2S_{inst}[r, t]$ curves corresponding to time-dependent I–I distance distribution functions of I_2 in cyclohexane. (b) Cross sections of $r^2S_{inst}[r, t]$ at the time delays indicated by dotted lines in (a). (c) Time evolution of the average I–I distance $<r(t)>$ was calculated from (a) and compared with a single exponential fit (red). The single exponential gives a satisfactory fit to the experimental data with a time constant of 55 ps.

I_2/CCl_4, the detailed time-dependent progression of the I–I distance is mapped out in the I–I distance distribution. At early times, the positive peak has a larger width, reaching larger distances than in I_2/CCl_4. This observation indicates that iodine atoms can be separated into larger distances in cyclohexane than in CCl_4. The average distance $<r(t)>$ is shown as a function of time in Figure 4c. A single-exponential function with a time constant of 55 ps provides a satisfactory fit to the decay profile. As both the population decay of the A/A′ state and the vibrational cooling are included in $<r(t)>$, the single-exponential behavior of $<r(t)>$ suggests that both processes have similar time constants and single-exponential decay profiles. As discussed above, Harris et al.[16] also reported that the decay of the A/A′ state is on the same time scale as the vibrational cooling process in cyclohexane. However, unlike in CCl_4 where the $<r(t)>$ value converges to 2.67 Å within 400 ps, $<r(t)>$ has not reached this equilibrium value in cyclohexane. This delay in reaching the equilibrium I–I distance may

dx.doi.org/10.1021/ja312513w | J. Am. Chem. Soc. 2013, 135, 3255–3261

indicate that the 55 ps process is the fast phase of a biexponential relaxation. This time constant of 55 ps is considerably slower than 16 ps observed in CCl_4.

The difference in the maximum I−I separation and the time scale of the vibrational cooling process in CCl_4 and cyclohexane can be explained by the difference in molecular mass of the two solvents. Cyclohexane is lighter than CCl_4, and as the iodine atoms move away from each other with bond elongation, they experience a smaller resistance force in cyclohexane than in CCl_4. As a result, the elongation of the I−I bond will reach larger distance (and the geminate recombination takes longer) in cyclohexane than in CCl_4.

3.4. Solute−Solvent Structural Dynamics. In addition to the change in bond length of solute molecules, we can also extract the solvation dynamics from the time-resolved X-ray liquidography data. In Figure 5a, the experimental $r^2\Delta S_{inst}[r, t]$ curves are plotted at large r values from 5.0 to 9.0 Å. This data corresponds to the time-dependent solute−solvent (mostly I−Cl) distance distribution in the distance regime of the first solvation shell surrounding the iodine molecule. For comparison, we performed a series of MD simulations of the I_2 molecule in CCl_4, of which the details are described in the Supporting Information. For each simulation, we fixed the I−I bond length to be a constant and performed many simulations while varying the I−I bond length. As a result, we obtained the pair distribution functions between atoms in solute and solvent molecules (that is, I−C and I−Cl) at various I−I bond lengths of the solute molecule and converted them to the difference distance distribution of the cage term, $r^2\Delta S_{cage}[r]$, as shown in Figure S19 (Supporting Information). Then, on the basis of the distribution of the I−I bond length of the solute molecule (in the range 2.3−4.2 Å) extracted from the experimental $r^2S_{inst}[r, t]$ in Figure 3a, we obtained the change of the theoretical solute−solvent distance distribution (i.e., cage term) as a function of time, as shown in Figure 5b. As can be seen in Figure 5a,b, the experiment and simulation show remarkably good agreement. In Figures 5c and 5d, we show examples of I−Cl and I−C pair distribution changes obtained from the MD simulation. As the I−I bond length of the I_2 molecule changes from 2.65 to 4.0 Å and from 2.65 to 3.1 Å, the I−Cl and I−C pair distribution functions change significantly, giving an oscillatory difference distribution. As schematically described in Figure 5e, the positive peaks at ∼7.7 Å (I−Cl distance in Figure 5c) and ∼8.5 Å (I−C distance in Figure 5d) represent the relatively increased population of longer solute-solvent distance distribution, which reflects the expanded solvation shell induced by the elongation of the I−I bond in I_2. On the other hand, the negative peaks at ∼6.0 Å (I−Cl distance in Figure 5c) and ∼7.0 Å (I−C distance in Figure 5d) reflect the depletion of the solute-solvent distance distribution in the ground-state configuration. Thus, we can infer that the first solvation cage expands by ∼1.5 Å along the I−I axis accompanying the elongation of I−I bond from 2.65 to 4.0 Å.

Previously, the solvation dynamics associated with the relaxation of electronic excited states were measured using spectroscopic methods such as time-resolved fluorescence Stokes shift,[1] photon echo,[2] and pump−probe[3,4] techniques, and the dynamics and the spectral signatures of solute−solvent interaction were elucidated. However, the signals measured by those spectroscopic techniques do not give direct information on the evolution of solute−solvent distances. In contrast, the interatomic distance distribution presented in this work is a direct real-space representation of the spatial rearrangement of the solvent molecules in the first solvation shell with respect to the solute molecules.

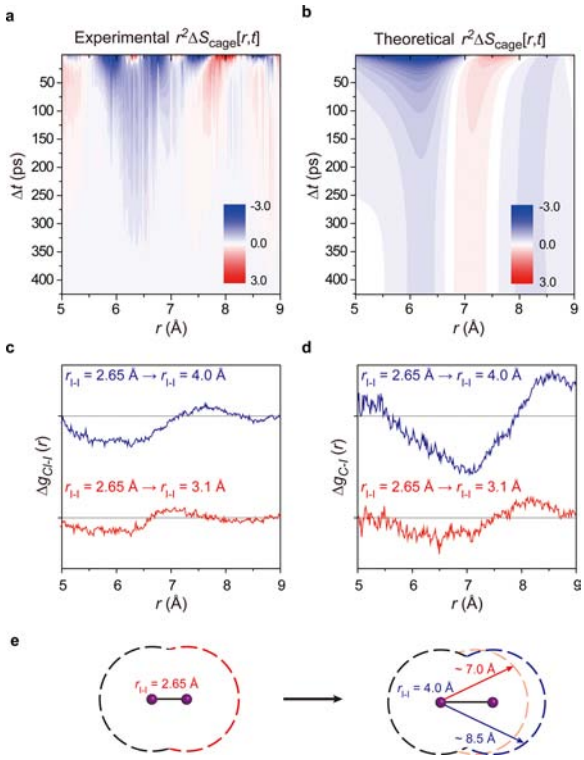

Figure 5. Time-dependent solute−solvent distance distribution functions ($r^2S_{inst}[r, t]$). (a) Experimental $r^2S_{inst}[r, t]$ curves at large r values corresponding to time-dependent solute−solvent (mostly I−Cl) distance distribution functions. (b) Theoretical time-dependent solute−solvent distance distribution functions based on the experimentally obtained I−I distribution (shown in Figure 3a) and the solute−solvent distance distribution functions at various I−I bond lengths from the MD simulation (Supporting Information, Figure S19). (c,d) Examples of the difference of the I−Cl pair distribution functions, $\Delta g_{Cl-I}(r)$, and the difference of the I−C pair distribution functions, $\Delta g_{C-I}(r)$, obtained from the MD simulation. The blue and red curves are for I−I distance changes from 2.65 to 4.0 Å and 2.65 to 3.1 Å, respectively. (e) Schematic for the change of the solvation shell due to the elongation of the I−I distance. Dotted circles indicate the first solvation shell. The interatomic distance shown in this figure is the distance between the I atom of the solute molecule and the C atom in the solvation shell. Because a CCl_4 molecule has one C atom surrounded by four Cl atoms and the Cl atom scatters much more strongly than the C atom, the scattering signal is dominated by the I−Cl contribution. Nevertheless, with the C atom being located at the center of the CCl_4 molecule, the I−C distribution provides a more intuitive picture of the size of the solvation shell.

4. CONCLUSION

In this study, by realizing the new technique of time slicing and deconvolution, we measured the dynamics of geminate recombination and vibrational relaxation of I_2 in two different solvents, CCl_4 and cyclohexane, in real time using picosecond X-ray liquidography. The birth and vibrational relaxation of I_2 molecules as well as the collective motions of the surrounding solvent molecules are visualized in real space in the form of time-dependent interatomic distance distribution functions. The results show that iodine atoms can be separated by larger distances in cyclohexane than in CCl_4 and the vibrational relaxation of a newly born "hot" I_2 molecule occurs faster in

dx.doi.org/10.1021/ja312513w | J. Am. Chem. Soc. 2013, 135, 3255−3261

CCl_4 than in cyclohexane. In addition to the structural progression of the solute molecule, the concomitant swelling and shrinking of the solute−solvent cage were also clearly observed. In general, molecular formation in solution occurs when two atoms (or molecules) belonging to different solvation cages meet each other and form a chemical bond while being merged into a single solvation cage. In contrast, geminate recombination of iodine atoms occurs only in a single cage because the two iodine atoms that are photodissociated from an iodine molecule recombine with each other before escaping the solvent cage. In that sense, iodine formation can be viewed as the later stage of molecular formation in general systems. Our scheme of using time slicing and deconvolution can serve as a general approach to circumvent the temporal limit imposed by pulse duration and may help future applications. For example, when femtosecond X-ray pulses are used in the future, even faster dynamics approaching the attosecond time scale may be extracted using the time-slicing scheme.

■ ASSOCIATED CONTENT

Ⓢ Supporting Information

Descriptions of detailed experimental procedures, detailed step-by-step data analysis, and MD simulation. This material is available free of charge via the Internet at http://pubs.acs.org.

■ AUTHOR INFORMATION

Corresponding Author

wulff@esrf.fr; hyotcherl.ihee@kaist.ac.kr

Present Address

[○]Institut de Physique de Rennes, Université de Rennes1-CNRS, UMR 6251, 35042 Rennes, France.

Notes

The authors declare no competing financial interest.

■ ACKNOWLEDGMENTS

We acknowledge R. Vuilleumier, X. Rozanska, E. Pontecorvo, C. Gilles, and K. H. Kim for help and discussions in the early stages of the project. This work was supported by the EU grants FAMTO (HPRICT-1999-50004) and FLASH (FP6-503641). This work was supported by the Research Center Program (CA1201) of IBS (Institute for Basic Science) in Korea and the Creative Research Initiative (Center for Time-Resolved Diffraction) of MEST/NRF. J.P. and K.B.M. were supported by the Danish National Research Foundation

■ REFERENCES

(1) Jimenez, R.; Fleming, G. R.; Kumar, P. V.; Maroncelli, M. *Nature* **1994**, *369*, 471−473.

(2) de Boeij, W. P.; Pshenichnikov, M. S.; Wiersma, D. A. *Annu. Rev. Phys. Chem.* **1998**, *49*, 99−123.

(3) Lian, T.; Kholodenko, Y.; Hochstrasser, R. M. *J. Phys. Chem.* **1995**, *99*, 2546−2551.

(4) Park, S.; Kim, J.; Scherer, N. F. *Phys. Chem. Chem. Phys.* **2012**, *14*, 8116−8122.

(5) Mulliken, R. S. *J. Chem. Phys.* **1971**, *55*, 288−309.

(6) Kelley, D. F.; Abul-Haj, N. A.; Jang, D. J. *J. Chem. Phys.* **1984**, *80*, 4105−4111.

(7) Bergsma, J. P.; Coladonato, M. H.; Edelsten, P. M.; Kahn, J. D.; Wilson, K. R. *J. Chem. Phys.* **1986**, *84*, 6151−6160.

(8) Harris, A. L.; Brown, J. K.; Harris, C. B. *Annu. Rev. Phys. Chem.* **1988**, *39*, 341−366.

(9) Jonas, D. M.; Bradforth, S. E.; Passino, S. A.; Fleming, G. R. *J. Phys. Chem.* **1995**, *99*, 2594−2608.

(10) Nitzan, A. *Chemical Dynamics in Condensed Phases*; Oxford University Press: New York, 2006.

(11) Franck, J.; Rabinowitsch, E. *Trans. Faraday Soc.* **1934**, *30*, 120−130.

(12) Rabinowitch, E.; Wood, W. C. *Trans. Faraday Soc.* **1936**, *32*, 547−555.

(13) Rabinowitch, E.; Wood, W. C. *Trans. Faraday Soc.* **1936**, *32*, 1381−1387.

(14) Chuang, T. J.; Hoffman, G. W.; Eisenthal, K. B. *Chem. Phys. Lett.* **1974**, *25*, 201−205.

(15) Abul-Haj, N. A.; Kelley, D. F. *J. Chem. Phys.* **1986**, *84*, 1335−1344.

(16) Harris, A. L.; Berg, M.; Harris, C. B. *J. Chem. Phys.* **1986**, *84*, 788−806.

(17) Xu, X. B.; Yu, S. C.; Lingle, R.; Zhu, H. P.; Hopkins, J. B. *J. Chem. Phys.* **1991**, *95*, 2445−2457.

(18) Scherer, N. F.; Jonas, D. M.; Fleming, G. R. *J. Chem. Phys.* **1993**, *99*, 153−168.

(19) Xu, J.; Schwentner, N.; Chergui, M. *J. Chem. Phys.* **1994**, *101*, 7381−7387.

(20) Zadoyan, R.; Sterling, M.; Ovchinnikov, M.; Apkarian, V. A. *J. Chem. Phys.* **1997**, *107*, 8446−8460.

(21) Mukamel, S. *Principles of Nonlinear Optical Spectroscopy*; Oxford University Press: New York, 1999.

(22) Bargheer, M.; Dietrich, P.; Donovang, K.; Schwentner, N. *J. Chem. Phys.* **1999**, *111*, 8556−8564.

(23) Apkarian, V. A.; Schwentner, N. *Chem. Rev.* **1999**, *99*, 1481−1514.

(24) Helbing, J.; Chergui, M. *J. Chem. Phys.* **2001**, *115*, 6158−6172.

(25) Shen, Y. R. *The Principles of Nonlinear Optics*; John Wiley & Sons: New York, 2002.

(26) Ihee, H.; Lorenc, M.; Kim, T. K.; Kong, Q. Y.; Cammarata, M.; Lee, J. H.; Bratos, S.; Wulff, M. *Science* **2005**, *309*, 1223−1227.

(27) Kim, T. K.; Lorenc, M.; Lee, J. H.; Russo, M.; Kim, J.; Cammarata, M.; Kong, Q. Y.; Noel, S.; Plech, A.; Wulff, M.; Ihee, H. *Proc. Natl. Acad. Sci. U.S.A.* **2006**, *103*, 9410−9415.

(28) Cammarata, M.; Lorenc, M.; Kim, T. K.; Lee, J. H.; Kong, Q. Y.; Pontecorvo, E.; Lo Russo, M.; Schiro, G.; Cupane, A.; Wulff, M.; Ihee, H. *J. Chem. Phys.* **2006**, 124.

(29) Kong, Q. Y.; Wulff, M.; Lee, J. H.; Bratos, S.; Ihee, H. *J. Am. Chem. Soc.* **2007**, *129*, 13584−13591.

(30) Lee, J. H.; Kim, J.; Cammarata, M.; Kong, Q.; Kim, K. H.; Choi, J.; Kim, T. K.; Wulff, M.; Ihee, H. *Angew. Chem., Int. Ed.* **2008**, *47*, 1047−1050.

(31) Lee, J. H.; Kim, T. K.; Kim, J.; Kong, Q.; Cammarata, M.; Lorenc, M.; Wulff, M.; Ihee, H. *J. Am. Chem. Soc.* **2008**, *130*, 5834−5835.

(32) Cammarata, M.; Levantino, M.; Schotte, F.; Anfinrud, P. A.; Ewald, F.; Choi, J.; Cupane, A.; Wulff, M.; Ihee, H. *Nat. Methods* **2008**, *5*, 881−886.

(33) Kong, Q. Y.; Lee, J. H.; Plech, A.; Wulff, M.; Ihee, H.; Koch, M. H. J. *Angew. Chem., Int. Ed.* **2008**, *47*, 5550−5553.

(34) Vincent, J.; Andersson, M.; Eklund, M.; Wohri, A. B.; Odelius, M.; Malmerberg, E.; Kong, Q. Y.; Wulff, M.; Neutze, R.; Davidsson, J. *J. Chem. Phys.* **2009**, 130.

(35) Ihee, H. *Acc. Chem. Res.* **2009**, *42*, 356−366.

(36) Kim, T. K.; Lee, J. H.; Wulff, M.; Kong, Q. Y.; Ihee, H. *ChemPhysChem* **2009**, *10*, 1958−1980.

(37) Ihee, H.; Wulff, M.; Kim, J.; Adachi, S. *Int. Rev. Phys. Chem.* **2010**, *29*, 453−520.

(38) Kong, Q. Y.; Lee, J. H.; Lo Russo, M.; Kim, T. K.; Lorenc, M.; Cammarata, M.; Bratos, S.; Buslaps, T.; Honkimaki, V.; Ihee, H.; Wulff, M. *Acta Crystallogr., Sect. A: Found. Crystallogr.* **2010**, *66*, 252−260.

(39) Kong, Q.; Lee, J. H.; Kim, K. H.; Kim, J.; Wulff, M.; Ihee, H.; Koch, M. H. J. *J. Am. Chem. Soc.* **2010**, *132*, 2600−2607.

(40) Haldrup, K.; Harlang, T.; Christensen, M.; Dohn, A.; van Driel, T. B.; Kjaer, K. S.; Harrit, N.; Vibenholt, J.; Guerin, L.; Wulff, M.; Nielsen, M. M. *Inorg. Chem.* **2011**, *50*, 9329−9336.

(41) Malmerberg, E.; Omran, Z.; Hub, J. S.; Li, X. W.; Katona, G.; Westenhoff, S.; Johansson, L. C.; Andersson, M.; Cammarata, M.; Wulff, M.; van der Spoel, D.; Davidsson, J.; Specht, A.; Neutze, R. *Biophys. J.* **2011**, *101*, 1345−1353.
(42) Kim, T. W.; Lee, J. H.; Choi, J.; Kim, K. H.; van Wilderen, L. J.; Guerin, L.; Kim, Y.; Jung, Y. O.; Yang, C.; Kim, J.; Wulff, M.; van Thor, J. J.; Ihee, H. *J. Am. Chem. Soc.* **2012**, *134*, 3145−3153.
(43) Kim, J.; Lee, J. H.; Kim, J.; Jun, S.; King, K. H.; Kim, T. W.; Wulff, M.; Ihee, H. *J. Phys. Chem. A* **2012**, *116*, 2713−2722.
(44) Kim, K. H.; Muniyappan, S.; Oang, K. Y.; Kim, J. G.; Nozawa, S.; Sato, T.; Koshihara, S. Y.; Henning, R.; Kosheleva, I.; Ki, H.; Kim, Y.; Kim, T. W.; Kim, J.; Adachi, S.; Ihee, H. *J. Am. Chem. Soc.* **2012**, *134*, 7001−7008.
(45) Ibrahimkutty, S.; Wagener, P.; Menzel, A.; Plech, A.; Barcikowski, S. *Appl. Phys. Lett.* **2012**, 101.
(46) Haldrup, K.; Vanko, G.; Gawelda, W.; Galler, A.; Doumy, G.; March, A. M.; Kanter, E. P.; Bordage, A.; Dohn, A.; van Driel, T. B.; Kjaer, K. S.; Lemke, H. T.; Canton, S. E.; Uhlig, J.; Sundstrom, V.; Young, L.; Southworth, S. H.; Nielsen, M. M.; Bressler, C. *J. Phys. Chem. A* **2012**, *116*, 9878−9887.
(47) Neutze, R.; Moffat, K. *Curr. Opin. Struct. Biol.* **2012**, *22*, 651−659.
(48) Plech, A.; Wulff, M.; Bratos, S.; Mirloup, F.; Vuilleumier, R.; Schotte, F.; Anfinrud, P. A. *Phys. Rev. Lett.* **2004**, *92*, 125505.
(49) Henriksen, N. E.; Møller, K. B. *J. Phys. Chem. B* **2008**, *112*, 558−567.
(50) Bratos, S.; Mirloup, F.; Vuilleumier, R.; Wulff, M. *J. Chem. Phys.* **2002**, *116*, 10615−10625.
(51) Janson, P. A. *Deconvolution with Applications in Spectroscopy*; Academic Press: New York, 1984.
(52) Wallace, W.; Schaefer, L. H.; Swedlow, J. R. *BioTechniques* **2001**, *31*, 1076−1097.
(53) Diaz-Zamboni, J. E.; Paravani, E. V.; Adur, J. F.; Casco, V. H. *Acta Microsc.* **2007**, *16*, 8−15.